Available online at www.sciencedirect.com
SCIENCE DIRECT
Physica D 215 (2006) 159–165
PHYSICA D
www.elsevier.com/locate/physd

Grouping behavior of inter-pulse time intervals for triggered pulses in an AlGaAs/InGaAs multilayer structure

A.B. Weerasekara, S.G. Matsik, G.S. Cymbalyuk, A.G.U. Perera*

Department of Physics and Astronomy, Georgia State University, Atlanta, GA 30303, United States

Received 12 September 2005; accepted 26 January 2006
Available online 13 March 2006
Communicated by R. Roy

Abstract

Triggered pulsing in a multi-quantum well structure which shows *s*-type negative differential resistance (NDR) was investigated. First return maps of the inter-pulse time intervals (IPTI) show an interesting grouping pattern at slower pulse rates. Oscillations in the pulsing threshold level of the MQW device cause the grouping behavior. This pattern of IPTIs is similar to that of thermoreceptors in fish and mammals. Correlation integrals were calculated for IPTI data sets collected under different operational conditions, and correlation dimensions 8.0, 8.0, 8.5, and 10.0 were found for four different data sets. The calculated correlation dimensions indicate that the triggered pulsing shows a high dimensional behavior and that the correlation dimension increases as the pulse rate decreases.

Keywords: Quantum well; Correlation dimensions; Chaos

1. Introduction

Development of an artificial neuron has been a challenge for the joint efforts of biologists, physicists, and electrical engineers for a long time [1]. Designing and fabricating artificial neurons with conventional electronics such as transistors and diodes may not be promising in terms of size and power requirements. Therefore, two-terminal semiconductor devices such as p^+–n–n^+ diodes and multilayer quantum well structures (MQW) which exhibit *s*-type current–voltage characteristics are of great interest as such devices can generate neuron-like pulses under suitable voltage or current bias [2,3]. *S*-type I–V characteristics [see Fig. 1(a)] of p^+–n–n^+ diodes and of MQW structures at low temperature (4.2–77 K) have been reported and studied by several researchers [4–6]. In general, the tunneling current is dominant in the lower branch of the I–V curve [see Fig. 1(a)] while thermionic current is dominant in the upper branch of the I–V curve. During the transition of the device current from the lower branch to the upper branch, the effective resistance in the device decreases with increasing current resulting in a negative differential resistance (NDR) region. With a suitable load resistor and a capacitor [see Fig. 1(b)], this type of device has shown neuron-like pulses [2,3] at low temperatures due to the bistability of the *s*-type I–V curve. This pulsing phenomenon has applications in the physics of devices such as artificial neurons [2,3] and IR detectors [7].

Several explanations for the *s*-type I–V behavior in semiconductor devices can be found in the literature [8–10]. Generally, impact ionization, impurities, and hot carrier transport are believed to be involved in this phenomenon. However, it is still a challenge to fabricate such devices consistently due to the lack of a complete model which takes the mechanism of the *s*-type behavior into account. According to reported *s*-type device designs, doping concentrations, well widths, barrier heights and widths, and impurities are critical for the NDR region. The other important factors could be the space charge accumulation at the interfaces of semiconductor layers [11] and defects in semiconductor materials.

In this study, a GaAs/$In_xGa_{1-x}As$ MQW structure grown by the molecular beam epitaxial technique (MBE), which has *s*-type I–V characteristics, was investigated in an effort to understand the pulsing phenomenon. Spontaneous pulsing in p^+–n–n^+ devices has shown a rich nonlinear behavior under

* Corresponding author. Tel.: +1 404 651 2709.
E-mail address: uperera@gsu.edu (A.G.U. Perera).

0167-2789/$ - see front matter © 2006 Elsevier B.V. All rights reserved.
doi:10.1016/j.physd.2006.01.020

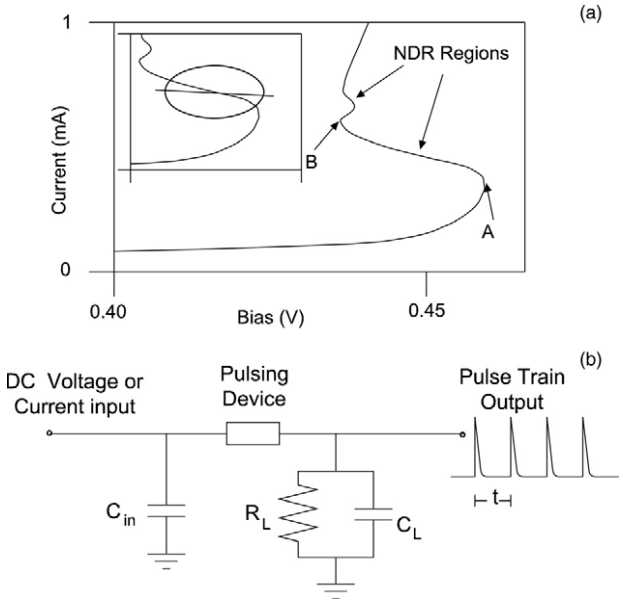

Fig. 1. (a) Current–voltage characteristics for the pulsing MQW device at $T = 4.2$ K. The negative differential region (NDR) is from A to B. There is another smaller NDR region above the main one. Region A to B corresponds to the unstable current and pulsing. The inset shows the load line (solid straight) and the path of device bias voltage and current during a pulse (oval). The device has the s-type I–V characteristic below $T = 23$ K. (b) The basic pulse mode circuit diagram. An input capacitor C_{in} (0.6 μF), a load capacitor C_L (0.11 μF), and a load resistor R_L (11.5 kΩ) are used in the circuit to work in the pulse mode. The device can be driven either in DC voltage bias or DC current bias mode.

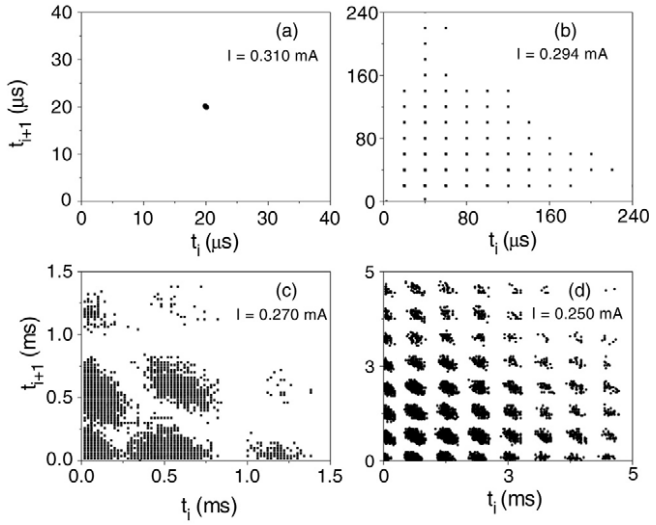

Fig. 2. The first return maps for different bias currents. (a) At $I_b = 0.310$ mA, all IPTIs are the same as that of the triggering signal which is 20 μs. (b) At $I_b = 0.294$ mA, IPTI has several values but all are multiples of the triggering signal period. (c) At $I_b = 0.270$ mA, formation of the first couple of groups can be seen. The time separation among groups is ∼0.5 ms. (d) At $I_b = 0.250$ mA, the pulsing rate is quite slow. There are more groups and they are clearly distinguishable. The time separation among groups is now ∼0.8 ms.

different operational conditions and has been studied before [11,12]. Preliminary studies on IPTIs based on power spectra and first return maps showed that the IPTIs of the MQW device possessed nonlinear behavior. Estimations for the correlation dimension and phase space dimension that could help in understanding the phenomena were also investigated.

2. Experimental set-up

The MQW device used in this study consists of 20 periods of 338 Å GaAs barriers and 83 Å $In_{0.087}Ga_{0.913}As$ wells. The I–V characteristic of the MQW device is shown in Fig. 1(a). The device shows the NDR characteristic below 23 K. However, the NDR region shifts upward with increasing temperature and the width of the NDR region shrinks. Above 23 K, the s-type I–V behavior disappears. The MQW device was operated in a simple circuit as shown in Fig. 1(b) and a rectangular pulse train with pulse amplitude of 10 mV and width of 2 μs was applied in order to trigger pulses. The amplitude of triggered pulses is approximately 40 mV at 4.2 K and decreases with increasing temperature. The triggered pulses were amplified and fed into a Lecroy 2323 programmable dual gate TTL output generator to produce TTL signals corresponding to the input signals. The TTL output signals were fed into a National Instrument PCI 6602 Counter Timer board to measure the time intervals between consecutive TTL signals which were IPTIs of triggered pulses. A Wavetek (Model 275) function generator was used as the triggering signal generator. IPTIs were collected under different device operating conditions such as device temperature, bias voltage or current, and triggering signal frequency.

3. First return maps

First return maps of IPTIs at different bias currents and voltages were used to analyze the nonlinear behavior of IPTIs. The general behavior of IPTIs with decreasing bias current is shown in Fig. 2. The following development in the first return maps can be clearly seen. When the bias current is near the transition current (point A) as shown by the I–V curve in Fig. 1(a), the device responds to each and every triggering voltage signal by producing a pulse. Therefore, each IPTI is as long as the IPTI of the triggering voltage signal and, hence, the first return map shows only a single point (see Fig. 2(a)). As the bias current moves from the transition point A to a lower value, the ability of the device to respond to each and every triggering voltage signal decreases due to the electric field across the device being smaller than in the earlier case. Therefore, IPTIs take a range of values giving rise to a different types of first return maps. The first return map for 0.294 mA bias current shows several IPTI values, as seen in Fig. 2(b). However, all IPTIs are multiples of the 20 μs triggering signal period. Further decreasing the bias current leads to an intriguing development in first return maps; i.e. grouping of IPTIs forms as seen in Fig. 2(c) and 2(d). As the bias current decreases further, more and more groups develop. Initially, the time separation among the groups (from center to center) is 0.5–0.6 ms (see Fig. 2(c)). When it reaches a state similar to that of Fig. 2(d), the time separation between consecutive groups is about 0.7–0.8 ms. When the bias current is so small that the triggering signal can barely trigger pulses, the second layer of groups emerges

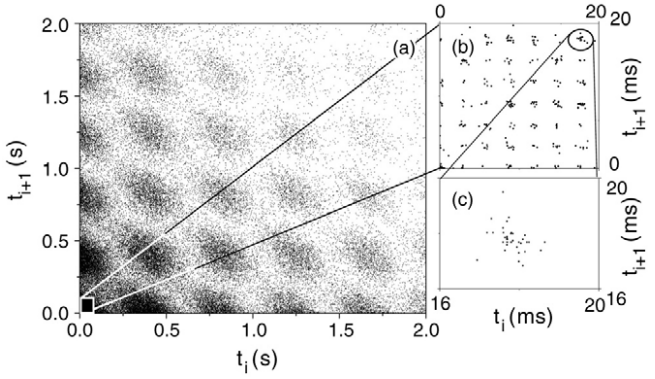

Fig. 3. (a) Larger groups at low bias voltage. Each larger group is made of 8000–10 000 smaller groups that are similar to the groups in Fig. 2. The time separation (from center to center) among larger groups is roughly ∼400 ms. (b) An expanded portion of the 0–20 ms area; the smaller groups can be clearly seen in it. Time separation among the smaller groups: ∼3 ms. A single smaller group is shown in (c). However, it is less populated because the same number of data points have been distributed over a very large number of groups.

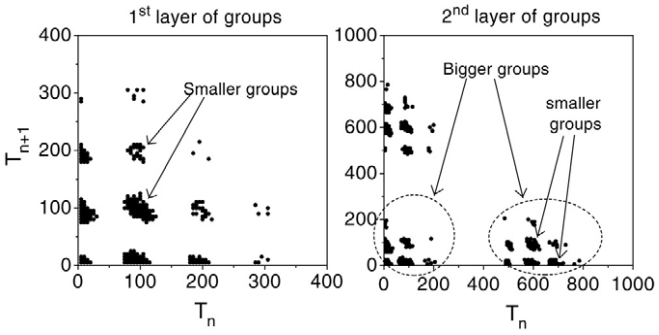

Fig. 4. Illustrates how the grouping occurs when the device threshold level fluctuates. (a) IPTI pattern after introducing $I_0 \sin(\frac{2\pi t}{T_0})$ to the threshold and for period $T_0 = 100$. Smaller groups can be clearly seen and it resembles the first layer of groups. (b) First return maps of IPTIs after introducing $I_0 \sin(\frac{2\pi t}{T_0}) + I_1 \sin(\frac{2\pi t}{T_1})$. Period $T_0 = 100$ and period $T_1 = 1000$. This resembles the second layer of groups. There are three bigger groups which are made up of smaller groups (the first layer of groups). Arbitrary dimensionless frequencies were selected for simplicity and white noise was introduced to make the first return map somewhat similar to the experimental ones.

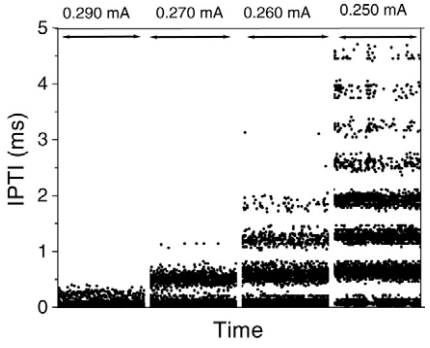

Fig. 5. IPTI band formation with decreasing device bias current. At $I = 0.290$ mA, only one band of IPTIs is possible; IPTI is roughly below 0.4 ms. When the bias current reaches 0.270 mA, IPTIs show splitting and give two types of IPTI bands. When the bias current reaches 0.265 mA, The IPTI undergoes one more splitting, giving three bands of IPTIs. As the bias current keeps decreasing, more and more IPTI bands develop.

and these new groups are large and made up of the first layer of groups (see Fig. 3(a). If one of these larger groups is enlarged, the first layer of groups is visible, as seen in Fig. 3(b). Generally, 8000–10 000 smaller groups can be found in a single larger group. The number of points in each smaller group is now less because points are distributed among thousands of smaller groups; therefore, smaller groups are not as clear as previous smaller groups seen in Fig. 2(d). The separation between larger groups is ∼400 ms while the separation between smaller groups has increased to ∼3 ms. This shows that the time interval among smaller groups changed from roughly 0.5 ms to 3 ms when the pulsing rate decreased.

The groupings are clearly seen for triggering signal frequencies 10, 20, 25, 40, and 50 kHz and cannot be clearly detected for some other frequencies, such as 11, 15, 18, and 30 kHz. However, the data point density variation in the first return maps for triggering signal frequencies 11, 15, 18, and 30 kHz revealed that groups exist but overlap with each other. The grouping behavior can be observed not only under current bias but also under voltage bias. Characteristics of grouping are the same for both current bias and voltage bias conditions.

This grouping can be associated with oscillations of the device threshold level. The first layer of groups can be empirically modeled by introducing a sinusoidal fluctuation, $I_0 \sin(\omega_0 t)$ to the constant threshold level of the device, I_{thresh}. The first return map of the simulated IPTIs shown in Fig. 4(a) clearly shows the first layer of groups. The second layer of groups can be obtained by introducing a second low frequency sinusoidal fluctuation to the device threshold, giving total threshold $I_{\text{thresh}} + I_0 \sin(\omega_0 t) + I_1 \sin(\omega_1 t)$. The corresponding first return map is shown in Fig. 4(b) and the second layer of groups can be seen. There are three larger groups and each larger group consists of smaller groups. Introducing white noise to the system produces IPTIs which give first return maps similar to the experimental ones. Space charge fluctuation in the device and small temperature fluctuations can lead to noise. The threshold oscillation frequency can be obtained from first return maps. According to the first return maps of the experimental data (Fig. 2(c,d)), the first layer of groups corresponds to high frequency oscillations which vary roughly from 0.35 to 2 kHz with decreasing applied bias current and the second layer of grouping corresponds to the low frequency oscillation, which is about 2 Hz according to the first return map (Fig. 3). Both bulk GaAs and GaAs superlattice structures are known for propagating charge domains [13–15]. These moving charge domains can produce current oscillations in the MQW device. Therefore, the pulsing threshold level of the MQW device can fluctuate accordingly.

The meaning of the groupings is that there are allowed and forbidden time bands for IPTIs. The development of the IPTI bands is shown in Fig. 5 at four different bias currents: $I_{\text{bias}} = 0.290$, 0.270, 0.260, and 0.250 mA. At the bias current $I_{\text{bias}} = 0.290$ mA, there is only one band, which is about 0.4 ms in width. When bias current decreases to $I_{\text{bias}} = 0.270$ mA, the second band develops, which is separated by a roughly 0.2 ms gap. IPTIs develop into four and eight bands at $I_{\text{bias}} =$

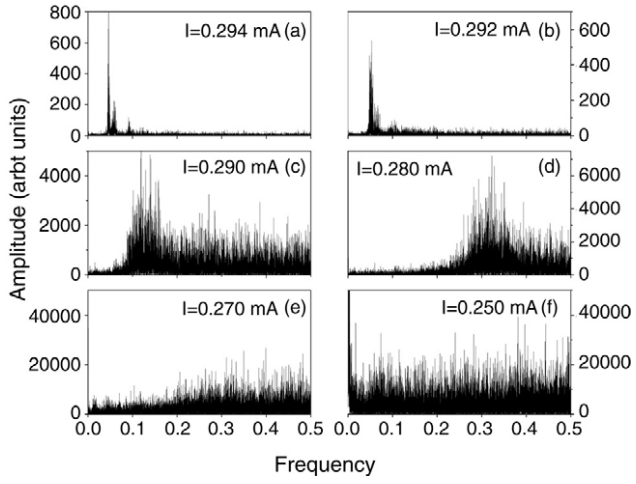

Fig. 6. Power spectrum development in IPTS's as bias current decreases. (a) At $I_b = 0.294$ mA, peaks of $\frac{1}{25}, \frac{1}{16}$ and its first harmonic can be seen. (b) At $I_b = 0.292$ mA, the frequencies of the peaks have increased by a small amount and become broader. (c), (d) Further decrease in bias current leads to a single broader peak. Formation of groups starts at this level. (d), (e) At very low bias current, the power spectra become much broader and complex. Well developed groups can be seen in the corresponding first return maps [see Fig. 3].

0.260 mA and $I_{\text{bias}} = 0.250$ mA respectively. With decreasing bias current, more and more IPTI bands can be seen. As more bands develop, the width of the bands decreases slightly and the separation between bands increases slightly. The IPTI band development is somewhat similar to bifurcation.

Although the first return maps show a clear pattern of IPTIs, according to the power spectra, there is no visible temporal pattern in IPTIs when groups develop. The evolution of the power spectra with decreasing bias current is depicted in Fig. 6. At bias current $I_{\text{bias}} = 0.294$ mA [see Fig. 6(a)], two very long periodic patterns can be seen, with frequencies of roughly $\frac{1}{25}$ and $\frac{1}{16}$ and the first harmonic of $\frac{1}{16}$. At bias current $I = 0.292$ mA, the peaks in the power spectrum as seen in Fig. 6(b) are not as sharp as those in Fig. 6(a) but are slightly broader. However, grouping has not yet started at these bias currents. As the bias current decreases, grouping starts slowly, the main peak gets broader and broader and the frequency gets larger and larger as seen in Fig. 6(c,d). Further decrease in bias current leads to complex and broader spectra as in Fig. 2(e,f) and well developed groups can be seen in first return maps as in Fig. 2(d). There is no clear temporal pattern in IPTIs according to the power spectra. The change of the power spectra from a long periodic line spectrum to a broad spectrum with decreasing bias current suggests nonlinear behavior.

4. Estimation of correlation dimension

Knowledge of the dimensionality of the system helps us understand the system operation and parameters which are responsible for the NDR region, including space charge build-up inside the device. Furthermore, it could help develop a model that can predict pulse patterns. The correlation dimension, D_2, can give a good understanding of the dimensionality of a nonlinear system. Grassburger and Procaccia presented a convenient method [16] for calculating the correlation dimension, D_2, from a single time series. They have shown that the correlation integral, $C(R)$, can be calculated as follows:

$$C(R) = \frac{1}{N^2} \sum_{i=1}^{N} \sum_{j=1}^{N} \Theta[R - (\overrightarrow{X_i} - \overrightarrow{X_j})] \tag{1}$$

where $\overrightarrow{X_i}, \overrightarrow{X_j}$ are ith and jth m-dimensional embedded vectors made of discrete measurements of the time series, R is the scaling region, N is the number of data and

$$\Theta[R - (\overrightarrow{X_i} - \overrightarrow{X_j})] = 0 \qquad \text{if } R \leq (\overrightarrow{X_i} - \overrightarrow{X_j}) \tag{2}$$

$$\Theta[R - (\overrightarrow{X_i} - \overrightarrow{X_j})] = 1 \qquad \text{if } R > (\overrightarrow{X_i} - \overrightarrow{X_j}). \tag{3}$$

Furthermore, they have shown that the correlation integral, $C(R)$ behaves as a power ν of R for small R:

$$C(R) \propto R^{\nu} \tag{4}$$

and the correlation dimension, D_2,

$$D_2 \approx \nu \tag{5}$$

where $C(R)$ is the correlation integral and given by Eq. (1), and R is called the scaling region. The correlation dimension, D_2, can be found by calculating the slope of $\ln(C(R))$ versus $\ln(R)$ in the linear scaling region. The scaling region, R, should be carefully picked so that the slopes of $\ln(C(R))$ versus $\ln(R)$ for different embedded dimensions should remain constant after a certain embedded dimension. Generally, this method is popular because it is accurate and fast. Sauer [17] has shown that the above method can be used for point processes such as measurements of time intervals between events. IPTI measurements in this experiment are also point processes and Eq. (1) can be used to investigate the correlation dimensions.

Using Eq. (1), the correlation integrals, $C(R)$, for different sets of IPTIs were calculated for different scaling regions, R, and for different embedded dimensions, m, and then $\ln(C(R))$ versus $\ln(R)$ was plotted and slopes in the best linear regions were found for different embedded dimensions, m. Finally those slopes were graphed against the embedded dimension, m. If the slopes reached a plateau after a certain embedded dimension, m, then the average value of the plateau was taken as an estimation of the correlation dimension, D_2. Table 1 gives the estimated correlation dimensions, D_2, for four data sets that shows converging slopes with increasing embedded dimension, m.

The calculated D_2 versus m for the above four data sets is shown in Fig. 7. The correlation dimension, D_2, for SET-1 converges to a value of 8.5 after the embedded dimension, m, reaches ~20 as seen in Fig. 7(a). In general, if D_2 converges, then it starts converging when $m \geq D_2$ [18]. In some cases, it can happen when $m \sim 2D_2$ [19]. Here, in this case, the plateau starts around $m \sim 20$, and it is roughly equal to $2D_2$. The bias current in this situation is close to the transition current [see Fig. 1]; therefore, the IPTIs are only a couple of times the triggering signal period and there is no grouping in the first return map. The power spectrum of SET-1 has two very long periodic patterns, one with a frequency of roughly $\frac{1}{160}$ and its

Table 1
Four data sets that showed converging correlation dimension, D_2

Data set	Bias	Temp. (K)	f_{trig} (kHz)	Number of data	D_2
SET-1	$V = 3.84$ V	4.2	50	200 000	8.5
SET-2	$I = 0.315$ mA	12	20	200 000	10
SET-3	$I = 0.300$ mA	10	10	150 000	8
SET-4	$I = 0.300$ mA	10	15	150 000	8

The data were collected under different operational conditions such as voltage bias and current bias, temperature, triggering signal frequency, f_{trig}.

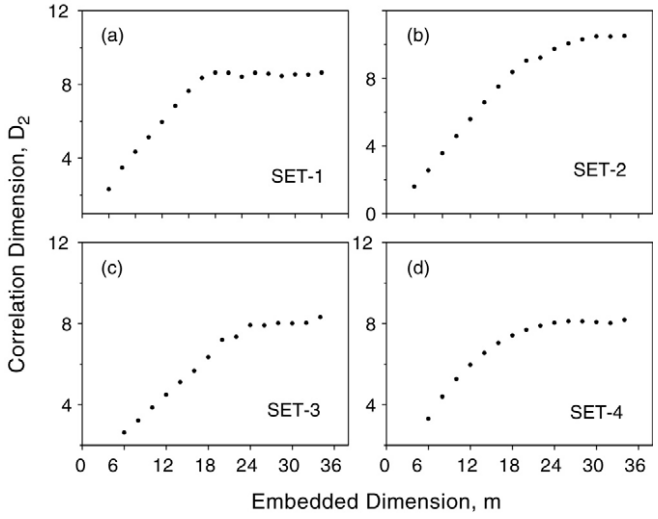

Fig. 7. The correlation dimension, D_2, versus the embedded dimension, m. The convergence of the correlation dimension, D_2, starts roughly at $m = 20$. (a) For SET-1, $D_2 \sim 8.5$. (b) For SET-2, $D_2 \sim 10.0$. (c) For SET-3, $D_2 \sim 8.0$. (d) For SET-4, $D_2 \sim 8.0$.

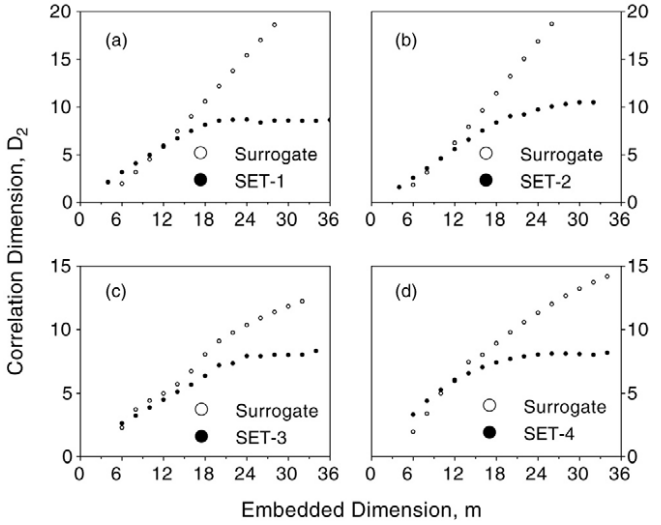

Fig. 8. The correlation dimension, D_2, versus the embedded dimension, m, for the surrogate data and original data. The correlation dimension, D_2, of the surrogate data does not converge, while the original data does, indicating the determinism associated with the original data.

first harmonic, the second one with a frequency of roughly $\frac{1}{55}$. The calculated autocorrelation for SET-1 is very small and less than $|0.2|$. Therefore, there is neither a strong correlation nor a random behavior.

Correlation dimensions, D_2, against embedded dimension, m, for SET-2 are shown in Fig. 7(b). The device temperature, bias current and the triggering signal frequency are 12 K, 0.315 mA, and 20 kHz respectively. The correlation dimension, D_2, converges to $\simeq$10. The corresponding first return map of SET-2 is shown in Fig. 3 with well developed groups in it. All those larger groups are formed by the smaller groups as explained in Section 3. The corresponding power spectrum has a broad spectrum suggesting that there is no simple temporal pattern associated with the IPTIs. The calculated autocorrelation function for SET-2 does not show a strong autocorrelation in IPTIs. It starts from approximately 0.06 and drops to zero after a time lag of 14 000.

The variations of the correlation dimension, D_2, with the embedded dimension, m, for SET-3 and SET-4 collected under the same operational conditions as are given in Table 1 except for the triggering signal frequency are shown in Fig. 7(c,d). Both sets converge towards the correlation dimension, D_2, of 8.0 when the embedded dimension, m, is greater than 20. The corresponding first return maps for both sets have no grouping because $I_{\text{bias}} = 0.30$ mA is fairly close to the transition current at the operating temperature $T = 10$ K, and IPTIs are only a few times the triggering signal period.

The convergence of D_2 in the above data sets is reasonably good. The corresponding power spectra and autocorrelations suggest that the data sets have neither strong correlation nor a randomness in IPTIs which can give a spurious correlation dimension, D_2. Furthermore, a surrogate data study was carried out to confirm the nonlinearity of IPTIs and the validity of the calculated correlation dimension, D_2. In general, surrogate data are generated using the original time series so that the surrogate data has the same statistical and power spectrum characteristics as the original time series has, but it has no deterministic properties. Therefore, the correlation dimension, D_2, for the surrogate data keeps increasing with increasing embedded dimension, m. For this study, surrogate data were generated according to the amplitude adjusted Fourier transformation (AAFT) algorithm [20] for each data set in Table 1 and, thereafter, correlation dimensions D_2 were calculated for generated surrogate data sets. The correlation dimensions D_2 of the original data sets and surrogate data sets were compared. They clearly show that while correlation dimensions D_2 of the original data converge, the correlation dimensions D_2 of the corresponding surrogate data do not, and they keep increasing as shown in Fig. 8. If the correlation dimension D_2 of the original data keeps increasing with increasing embedded dimension m, the data are not deterministic. If the correlation dimension D_2 of the surrogate data converges to some value with increasing embedded dimension m, both the original data

and the surrogate data would produce a spurious correlation dimension, D_2. In this test, the correlation dimension D_2 of the surrogate data does not converge. Thus, the surrogate data studies and the original data studies confirmed the deterministic nature of IPTIs obtained from experiments.

5. Discussion

First return maps show an interesting feature, the grouping of IPTIs. Grouping starts to appear on first return maps when the pulse rate is slower. This grouping is clearly seen when the triggering signal frequency is 10, 20, 25, 40, and 50 kHz; it is not quite visible for frequencies such as 11, 15, 18, and 30 kHz and the groups are smeared out. Oscillation of the threshold level of the MQW device can lead to this grouping behavior, as shown in Section 3. The threshold oscillation frequency changes roughly from 0.3 to 2 kHz with decreasing bias current. Therefore, the oscillation frequency depends on the bias current. The resonance frequency in the circuit output branch is about 4.5 Hz, i.e., its period is roughly 200 ms whereas the high frequency oscillations of the threshold vary roughly from 350 to 2000 Hz, which gives the first layer of groups. Time separations among the second layer of groups (larger groups) are about 400–500 ms which is roughly 2 Hz. Therefore, there is no apparent circuit resonance frequency influencing the grouping formation. The characteristics of grouping did not change significantly with changes of the load resistor R_L and C_L.

A similar type of behavior in IPTIs from cold receptor neurons of cats with changing temperature was reported and IPTI band formation similar to that in Fig. 5 was presented [21]. Roughly six IPTI bands can be seen at the temperature of 35 °C. If the first return map of IPTIs is plotted, it will give several groups similar to our ones. Furthermore, this type of behavior in IPTIs of rat facial cold receptor neurons has also been reported [22]. It has been seen that IPTIs from the rat facial cold receptor neuron split (bifurcate) into two different bands of IPTIs with temperature. In the first return map of IPTIs, three groups can be clearly seen. This MQW device demonstrates a similar phenomenon with decreasing bias current. Even with increasing temperature, grouping behavior in IPTIs could be seen. If the bias current and triggering signal frequency were constant, while increasing the operational temperature slowly, at the beginning, the device would start responding with a faster pulse rate and would slow down as temperature increased, because the NDR region shifts up with increasing temperature, making the bias current a little further away from the transition current of the I–V curve. In other words, this situation is similar to the situation where the bias current is gradually reduced, as discussed in Section 3. Therefore, groupings of IPTIs with increasing temperature can be seen. The device and the cold receptor neuron show similar patterns of IPTI behavior.

The behavior of the driven pulse pattern under voltage bias does not show a significant difference from that of under current bias. Generally, the temporal pattern of IPTIs in p^+–n–n^+ under constant current bias [23,11] is different from that for constant voltage bias [24,25]. The MQW device can produce the same IPTI pattern irrespective of whether it is biased under constant current or constant voltage, provided that the biasing is large enough that total current is close to the transition current, at point A [see Fig. 1]. It shows grouping of IPTIs under smaller constant current bias as well as under smaller constant voltage bias.

Even though groups in first return maps are in good arrangement, there is no simple periodic pattern in the power spectra of corresponding IPTIs. There is a relationship among IPTIs since t_i and t_{i+1} are allowed to visit only selected regions in first return maps. Identifying that relationship would help develop an algorithm which can predict IPTIs.

According to the calculations, the correlation dimension D_2 is quite large and varies from 8 to 10. This means the dimension of the phase space can be between 8 and 10. In this study, several data sets were collected under different biases, temperatures, and triggering signal frequencies. Correlation dimensions D_2 were calculated for all data sets. However, only data sets shown in Table 1 demonstrated converging correlation dimension D_2 with increasing embedded dimension, m. Other data sets did not show convergence. Correlation dimensions of the data sets which were collected under the same operational parameters as for SET-1, SET-2, SET-3, and SET-4 except for one variable were carefully examined and did not show a trend with changing parameter. Surrogate tests were carried out to confirm the reliability of the calculated correlation dimensions D_2 and, in addition, calculated autocorrelation of IPTIs reveals a weak correlation among IPTIs. As a whole, the correlation dimension D_2 converges to fairly high values providing evidence of the high dimensionality. This could be another situation where high correlation dimensions are reported [26,27]. Unfortunately, for practical reasons, we are unable to come to a conclusion as regards an exact correlation dimension within a reasonable error.

Acknowledgements

This work was supported in part by the NSF under Grant No. ECS-0140434. A.B. Weerasekara is partially supported by GSU Brain and Behavior program. The authors wish to thank Dr. V.E. Bondarenko for fruitful discussions.

References

[1] M. Mahowald, R.J. Douglas, Nature 354 (1991) 515.
[2] D.D. Coon, A.G.U. Perera, Solid State Electron. 31 (1986) 851.
[3] D.D. Coon, A.G.U. Perera, Neural Netw. 2 (1989) 143.
[4] M. Yin, P.M. Smowton, P. Blood, B. McAuley, C.C. Button, Solid State Electron. 45 (2001) 447.
[5] A.G.U. Perera, S.G. Matsik, V.Y. Letov, H.C. Liu, M. Gao, M. Buchanan, W.J. Schaff, Solid State Electron. 45 (2001) 1121.
[6] A. Reklaitis, A. Krotkus, A. Geiztis, M. Asche, Semicond. Sci. Technol. 14 (1998) 341.
[7] D.D. Coon, A.G.U. Perera, Solid State Electron. 29 (1986) 929.
[8] Zh.I. Alferov, O.A. Mexrin, M.A. Sinitsyn, S.I. Troshkov, B.S. Yavich, Sov. Phys. Semicond. 21 (1987) 304.
[9] A.G.U. Perera, S.G. Matsik, Appl. Phys. Lett. 67 (1995) 962.
[10] K. Hess, T.K. Higman, M.A. Emanuel, J.J. Coleman, J. Appl. Phys. 60 (1986) 3775.
[11] A.G.U. Perera, S.G. Matsik, Physica D 84 (1995) 615.

[12] D.D. Coon, A.G.U. Perera, Appl. Phys. Lett. 51 (1987) 1086.
[13] L. Esaki, L.L. Chang, Phys. Rev. Lett. 33 (1974) 495.
[14] B. Willing, J.C. Maan, Phys. Rev. B 49 (1994) 13995.
[15] J. Kastrup, F. Prengel, H.T. Grahn, K. Ploog, E. Scholl, Phys. Rev. B 53 (1996) 1502.
[16] P. Grassberger, I. Procaccia, Phys. Rev. Lett. 50 (1983) 346.
[17] T. Sauer, Phys. Rev. Lett. 72 (1994) 3811.
[18] M. Ding, C. Grebogi, E. Ott, T. Sauer, J.A. Yorke, Phys. Rev. Lett. 70 (1993) 3872.
[19] F. Takens, Detecting strange attractor in turbulence, in: Lecture Notes in Mathematics, vol. 898, Springer, Berlin, Germany, 1981, pp. 366–381.
[20] J. Theiler, S. Eubank, A. Longtin, B. Galdrikian, J.D. Farmer, Physica D 58 (1992) 77.
[21] W. Braun, B. Eckhardt, H.A. Braun, M. Huber, Phys. Rev. E 62 (2000) 6352–6360.
[22] F. Moss, L. Wilkens, X. Pei, K. Dolan, H.A. Braun, M.D. Lad, K. Schafer, K. Voigt, Finding unstable periodic orbits in physical and biological dynamical systems, in: Proceedings of the 4th Experimental Chaos Conference, 06–08 August, 1997, Florida, USA, World Scientific, 1997, pp. 289–301.
[23] D.D. Coon, A.G.U. Perera, Appl. Phys. Lett. 55 (1989) 478.
[24] K.M.S.V. Bandara, D.D. Coon, R.P.G. Karunasiri, Appl. Phys. Lett. 51 (1987) 961.
[25] D.D. Coon, A.G.U. Perera, Appl. Phys. Lett. 51 (1987) 1711.
[26] J.H. Chae, J. Jeong, B.S. Peterson, D.J. Kim, W.M. Bahk, T.Y. Jun, S.Y. Kim, K.S. Kim, Psychiatry Res. Neuroimaging 131 (2004) 79.
[27] J. Lamberts, P.L.C. Van Den Broek, L. Berner, J. Van Egmond, R. Dirksen, A.M.L. Coenen, Biol. Psychol. 41 (2000) 149–153.